The shape and parameters of the Lambda (1405) resonance

J. Phys. G: Nucl. Part. Phys. 17 (1991) 289–302. Printed in the UK

The shape and parameters of the Λ(1405) resonance

R H Dalitz† and A Deloff‡

† Department of Theoretical Physics, Oxford University, Oxford OX1 3NP, UK
‡ Institute for Nuclear Studies, Warsaw PL-00681, Hoza 69, Poland

Received 26 September 1990

Abstract. The experimental $\pi^-\Sigma^+$ mass spectrum for the reaction $K^-p \to \Sigma^+\pi^-\pi^+\pi^+$ at 4.2 Gev c^{-1} is fitted up to the K^-p threshold by a number of phenomenological models, using the M-matrix, the K-matrix and separable potentials in the $(\pi\Sigma, \bar{K}N)$ coupled channels. The best estimate for the mass of Λ(1405) is 1406.5 ± 4.0 MeV, with a full width of 50 ± 2 MeV, although there is some discordance between these models, each of which gives an acceptable fit to this spectrum.

1. Introduction

The $I = 0$ Λ(1405) peak has been known for a long time in the $(\pi\Sigma)^0$ spectra observed in final states following K^-p and πp interactions at high energy [1]. The largest body of data reported is that of Hemingway [2] from the K^-p reactions at 4.2 GeV giving $\pi^-(\Sigma^\pm\pi^\mp\pi^+)$, where he found that these $(\Sigma\pi\pi)^+$ states are dominated by the $I = 1$ resonance Σ*(1660). He selected events resulting from the well known $\Sigma^*(1660)^+ \to \pi\Lambda(1405)$ decay, thus

$$\Sigma^*(1660)^+ \to \pi^+\Lambda(1405) \begin{cases} \nearrow \pi^+ + \pi^- + \Sigma^+, & (1a) \\ \searrow \pi^+ + \pi^+ + \Sigma^-. & (1b) \end{cases}$$

Σ*(1660) is known to have $J^P = \frac{3}{2}^-$, while Λ(1405) has $J^P = \frac{1}{2}^-$, so that $l_\pi = 2$ holds for the primary π^+. The Λ(1405) has always been assigned to $J^P = \frac{1}{2}^-$ since the $\pi\Sigma$ mass spectrum has rapid variation with CM energy E in the vicinity of 1432 MeV, the mass of the K^-p threshold, which is attributed to a strong coupling of the $\pi\Sigma$ state with the K^-p S wave, the latter necessarily having $J^P = \frac{1}{2}^-$. All spin-parity tests on $\Lambda(1405) \to \pi\Sigma$ which have been made are consistent with this assignment and no data requires any other assignment.

The $\pi^+\Sigma^-$ mass distribution in the final state (1b) is distorted by the effects of Bose statistics for the two π^+ mesons. Hemingway therefore focused attention on the reaction (1a), having found that the $\pi^+\Sigma^-$ distribution for reaction (1b) is consistent with the distribution obtained by folding the $\pi^+\pi^-\Sigma^+$ plot (1a) across the axis of symmetry between π^+ and π^-. His mass distribution for $(\Sigma^+\pi^-)$ in (1a) is plotted in figure 1. We note that this distribution has a marked asymmetry about its peak since it falls rapidly as $M(\Sigma^+\pi^-)$ moves upward towards 1432 MeV. It cannot be satisfactorily represented by a Breit–Wigner resonance, as Hemingway noted. How then should this resonance state be represented adequately?

0954-3899/91/030289 + 14 $03.50

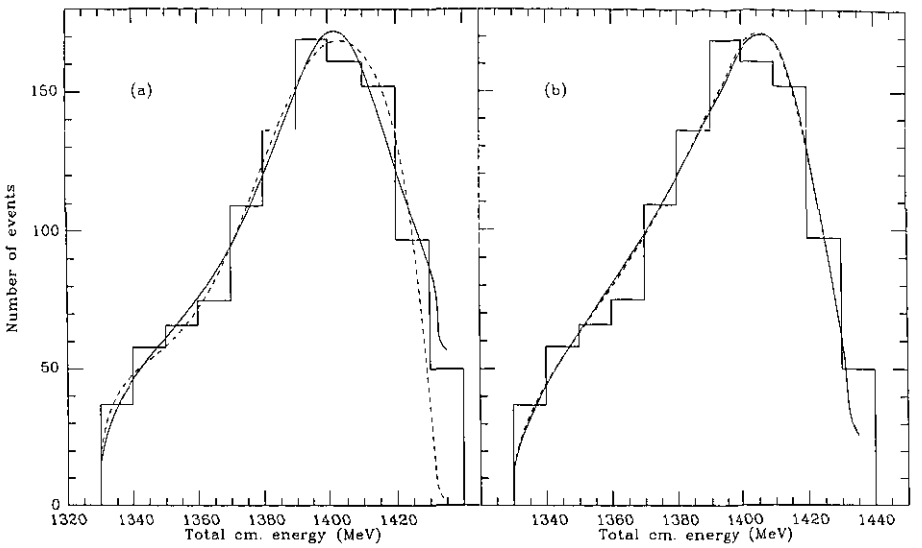

Figure 1. Hemingway's data on the $\pi^-\Sigma^+$ effective mass distribution [1], plotted in 10 MeV bins up to 1430 MeV. (*a*) shows our best fits for the *M*-matrix (full curve) and *K*-matrix (broken curve) parametrizations. (*b*) shows our best-fits for a Yamaguchi separable potential, SR (full curve) being that for relativistic kinematics and SNR (broken curve) being that for non-relativistic kinematics for both π and Σ. The SR and SNR fits are almost indistinguishable.

In section 2, we discuss the basis of our calculations, the use of the impulse approximation together with Watson's approximation to obtain the necessary matrix elements, and lay out three phenomenological models for these calculations, each leading to a $(\pi\Sigma)$ mass spectrum in terms of a number of parameters. In section 3, we show how we limit these parameters by several phenomenological constraints and we then calculate χ^2 as a function of an assumed resonance energy value E_R. We estimate the best value E_R and its error $\pm\sigma_R$ for each model from χ^2_{min} and the form of $\chi^2(E_R)$ around this minimum. In section 4, we discuss briefly the estimates of (E_R, Γ) from each model and the relative merits of these models. We conclude with a discussion of the data and theory needed for firmer determinations of the parameters for $\Lambda(1405)$.

2. The models

The approach used here is to appeal to the Watson approximation [3] for a final-state interaction. Watson pointed out that a two-particle wavefunction can be represented approximately by its asymptotic form for separations beyond the radius of their interaction. In this case, the two-particle wavefunction in a relative S-wave (the case of interest to us) has the asymptotic form

$$\psi(\boldsymbol{r}_1, \boldsymbol{r}_2) \propto \{\exp[i\boldsymbol{Q}\cdot(\boldsymbol{r}_1+\boldsymbol{r}_2)/2]\}\phi_{as}(r_{12})$$
$$= \{\exp[i\boldsymbol{Q}\cdot(\boldsymbol{r}_1+\boldsymbol{r}_2)/2]\}\sin(kr_{12}+\delta)e^{i\delta}/r_{12} \qquad (2)$$

where $\boldsymbol{r}_1$ and $\boldsymbol{r}_2$ are the position vectors of the two particles, $r_{12} = |\boldsymbol{r}_1 - \boldsymbol{r}_2|$, $\boldsymbol{Q}$ is their total momentum, k is the CM momentum and $\delta(k)$ is the scattering phaseshift. This

wavefunction is to be inserted in the impulse approximation matrix element describing the reaction leading to the final (1, 2) state of interest; the integral leads to an expression of the general form

$$\int F(1,2;\alpha)\exp[\mathrm{i}\boldsymbol{Q}\cdot(\boldsymbol{r}_1+\boldsymbol{r}_2)/2]\left(\frac{\sin kr_{12}}{kr_{12}}\cos\delta+\frac{\cos kr_{12}}{kr_{12}}\sin\delta\right)\mathrm{e}^{\mathrm{i}\delta}\,\mathrm{d}^3\boldsymbol{r}_1\,\mathrm{d}^3\boldsymbol{r}_2\prod_{\alpha}\mathrm{d}^3\boldsymbol{r}_\alpha \quad (3)$$

where α enumerates the other particles present and $F(1,2;\alpha)$ is a product of initial and final wavefunctions for all the particles, apart from the (1, 2) final-state wavefunction. If the (1, 2) interaction range is small relative to the size parameters occurring in the wavefunction product F, the second term, which is proportional to

$$\sin\delta\,\mathrm{e}^{\mathrm{i}\delta}/k \quad (4)$$

will provide a good approximation to the k dependence of the matrix element. This is particularly the case when the (1, 2) CM energies straddle a narrow resonance, so that $\delta(k)$ increases rapidly through $\pi/2$ as E passes through the resonance energy E_{R}. Here and later we shall *define* E_{R} to be the energy $E(k)$ for which $\delta(k)=\pi/2$. The question now becomes 'how should we represent $\delta(k)$ as a function of the (1, 2) CM energy?'

Much data has been obtained over the years on the scattering and reaction processes observed for the $\mathrm{K}^-\mathrm{p}$ system at low energies, especially at rest and for K^- laboratory momenta in the range 100–300 MeV c^{-1} (a summary of all these data will be given in [4]). This has been analysed many times and in various ways [4, 10, 20] usually in terms of a K-matrix parametrization [11]. This representation has been adopted because these interactions are very strong and it is essential the constraints of unitarity should be satisfied. This is especially the case for any energy range in which a strong two-body S-wave threshold occurs; the rate for transitions to the new channel rises rapidly with E, like $(E-E_{\mathrm{t}})^{1/2}$, where E_{t} denotes the threshold energy. Since S-matrix amplitudes have well defined analyticity properties as a function of energy E, this square-root singularity generally requires a strong energy dependence also just below this threshold. However, the K-matrix is defined in such a way [11] that it does not have a branch point at a two-particle threshold, but varies smoothly with energy across this S-matrix singularity at E_{t}. Use of a K-matrix therefore allows the possibility of describing simultaneously the behaviour in the physical regime $k_{\mathrm{Klab}}\sim 100$–300 MeV c^{-1} and at the thresholds $\mathrm{K}^-\mathrm{p}$ and $\bar{\mathrm{K}}^0\mathrm{n}$, which are separated by 5.32 MeV owing to electromagnetic mass differences which violate I-spin symmetry. Further, it can be used for E below E_{t}, where the $\bar{\mathrm{K}}\mathrm{N}$ state is non-physical but $\pi\Sigma$ elastic scattering is still a process physically possible. This requires an analytic continuation of the S-matrix into the domain $E<E_{\mathrm{t}}$, unphysical for the $\bar{\mathrm{K}}\mathrm{N}$ channel, and this is straightforward when the K-matrix is used. For an overall fit to all low-energy $\mathrm{K}^-\mathrm{p}$ interaction data, this makes it possible to include the below-threshold data on the $(\pi\Sigma)^0$ mass distribution. This extension is desirable, as these data below threshold lead to a more balanced constraint on the K-matrix parameters, and they have been taken into account in a number of recent $\bar{\mathrm{K}}\mathrm{N}$ analyses [4, 8, 20].

Our purpose in this paper is to determine the parameters for a fit to the shape of the $(\pi\Sigma)^0$ mass spectrum alone. Of course, in a sense, this fitting has already been done as part of these overall K-matrix fits. However, there is clearly a problem; in these overall fits, the $\Lambda(1405)\rightarrow\pi\Sigma$ data provide only 10 points in a total of about 261 data points, and the best fit obtained depends far more on the details of the

above-threshold data than on this below-threshold data. Indeed, these overall fits generally give a rather poor account of the $(\pi\Sigma)^0$ mass spectrum; the net $(\chi^2)_{\min}$ has relatively large contributions from these below-threshold data. This is clearly not a satisfactory situation, for the overall fit may be testing the validity of a simple K-matrix energy dependence rather than finding the proper parameters for $\Lambda(1405)$. We shall therefore fit the $(\pi\Sigma)^0$ data separately, but with the constraint that the parameters used must fit the known $I = 0$ $\bar{K}N$ scattering length at the K^-p threshold. This abstracts from the low-energy data analyses, one quantity which has varied relatively little through most of the $\bar{K}N$ data fitting since 1967 [5–10], we shall work with the value [4]:

$$a_0 + ib_0 = (-1.54 + i0.74)\text{fm}.$$

We have considered three models for this fit.

(a) The M-matrix fit, where $M(E)$ is the inverse of the $K(E)$ matrix:

$$M(E) = K(E)^{-1} = \begin{pmatrix} M_\Sigma(E_t) & M_X(E_t) \\ M_X(E_t) & M_N(E_t) \end{pmatrix} + (E - E_t)\begin{pmatrix} R_\Sigma & R_X \\ R_X & R_N \end{pmatrix}, \tag{5}$$

where E denotes the total CM energy, E_t the $\bar{K}N$ threshold energy, and R_Σ, R_N and R_X are constants. The suffices Σ and N refer to the channels $\pi\Sigma$ and $\bar{K}N$, while X refers to the $\bar{K}N \leftrightarrow \pi\Sigma$ transition. This is the form proposed first by Ross and Shaw [12] who derived it as an effective range theory, from rather general arguments. This form has special interest because it reduces, in the one-channel case and the non-relativistic limit, to the well known effective range theory for low-energy S-wave neutron–proton scattering [13]. The $^3S_1$ np system has the deuteron as bound state at energy $E = -2.2245$ MeV relative to the np threshold, and this effective range formalism provides an excellent account of both the deuteron and np scattering up to CM energy of order 20 MeV. In our case, there are two channels $\pi\Sigma$ and $\bar{K}N$ with different thresholds (1337 MeV and 1432 MeV, respectively), but there appears to be an unstable bound state in the system at energy about 24 MeV below the $\bar{K}N$ threshold. There is a considerable parallel between these two physical situations.

(b) An energy-dependent K-matrix fit

$$K(E) = \begin{pmatrix} K_\Sigma(E_t) & K_X(E_t) \\ K_X(E_t) & K_N(E_t) \end{pmatrix} + (E - E_t)\begin{pmatrix} \rho_\Sigma & \rho_X \\ \rho_X & \rho_N \end{pmatrix} \tag{6}$$

where ρ_Σ, ρ_N and ρ_X are constants. This form has no particular theoretical motivation. It is generally appropriate when the forces are only moderate in strength.

(c) A separable-potential model SR, with relativistic kinematics, given in momentum space by the Yamaguchi form,

$$\langle k | V_{ij} | k' \rangle = -(g_i(k) s_{ij} g_j(k'))/2\pi^2 \tag{7}$$

where the function $g(k) = (\beta_i^3/\mu_i)^{1/2}/(k^2 + \beta_i^2)$, μ_i being the reduced mass in channel i, and the s_{ij} denote the potential strengths. The normalization adopted makes the diagonal values strength parameters, i.e. when $s_{ii} \geqslant 1$, the potential V_{ii} acting alone leads in the non-relativistic case to a bound state in channel i. The motivation for this potential model is two-fold. Its parameters β_i^{-1} reflect economically the physical range of the potential, so that the reasonableness or otherwise of the β_i parameters is immediately apparent; the parameters R for the M-matrix and ρ for the K-matrix do not have this immediate interpretation. Further, the models determined for $\pi\Sigma$

scattering here are to be used in calculations of the properties of multiparticle reactions involving these particles, such as the K^-–deuteron reactions leading to $\pi\Sigma N$ final states [14]. Fadeev methods are conveniently practicable when particle–particle interactions can be represented by separable potentials. Indeed, this is the case *par excellence* if the particle kinematics can also be represented, at least approximately, by non-relativistic expressions, since the kinetic energy in two-particle subsystems can then be separated out from the kinetic energies involving other particles present. For this reason, we shall also investigate the separable non-relativistic case, which we denote by SNR.

Returning to model SR, the T-matrix in the $\pi\Sigma$ channel is, with (7)

$$T_\Sigma(E) = \frac{e^{i\delta}\sin\delta}{q} \tag{8a}$$

$$= \Omega_\Sigma(E)\left\{\frac{s_\Sigma - (s_\Sigma s_N - s_X^2)I_N}{1 - s_N I_N - s_\Sigma I_\Sigma + (s_N s_\Sigma - s_X^2)I_N I_\Sigma}\right\}, \tag{8b}$$

where E denotes the total CM energy

$$E = \omega_\pi(q)) + E_\Sigma(q)) = \omega_K(k) + E_N(k) \tag{9}$$

$$\Omega_\Sigma(E) = 2g_\Sigma(q)^2\omega_\pi(q)E_\Sigma(q)/E, \tag{10}$$

and $I_j(E)$ is the integral

$$I_j(p_j) = \frac{2\beta_j^3}{\pi\mu_j}\int_0^\infty \frac{p^2\,dp}{(p^2+\beta_j^2)^2}\cdot\frac{1}{(\omega_j(p)+E_j(p)-E-i\varepsilon)}, \tag{11}$$

expressible most conveniently in terms of channel momentum p_j. In the non-relativistic limit for both meson and baryon (the model SNR), this expression reduces to the form

$$I_j^{NR}(E) = (1 - ip_j/\beta_j)^{-2} \tag{12}$$

which also expresses (apart from a relativistic factor) the singular part of the fully relativistic expression (11), as is shown in the appendix. When the energy E lies below the threshold energy for channel j, the momentum p_j takes the value $+i|p_j|$, and (11) is no longer singular but takes the real form:

$$I_j^{NR}(E) = (1 + |p_j|/\beta_j)^{-2}. \tag{13}$$

Since the pion is certainly relativistic, we have simplified the integral (11) in our numerical work by taking the non-relativistic limit for the baryon only

$$E(p) = \omega(p) + M + p^2/2M \tag{14}$$

since this allows explicit analytic integration for $I_j(E)$, as discussed in the appendix. However, all expressions given in the body of this paper are valid for the fully relativistic case.

3. The fit to data

Each of the models described above has a number of parameters which are to be determined from the data. For this purpose, we have calculated the $\pi\Sigma$ scattering

cross sections for these models as a function of these parameters, subject to three constraints:

(i) that the $I=0$ $\bar{K}N$ scattering amplitude at threshold has the value $A_N(E_t) = (a_0 + ib_0)$ given by (4),

(ii) that the resonance energy has an assigned value E_R.

For the K-matrix model (6), these constraints are readily implemented. The $\bar{K}N$ scattering length is given generally by the form [11]

$$A_N(E) = K_N(E) + K_\Sigma(E)\frac{1}{1 - iqK_\Sigma(E)}iqK_\Sigma(E). \tag{15}$$

Its evaluation at $E = E_t$ allows the constraint (i) to be written in the form of two equations:

$$a_0 = -K_N(E_t) - q_t K_\Sigma(E_t) b_0 \tag{16a}$$

$$b_0 = q_t K_\Sigma(E_t)^2/(1 + q_t^2 K_\Sigma(E_t)^2), \tag{16b}$$

which determines $K_\Sigma(E_t)^2$ and $K_\Sigma(E_t)$ in terms of $K_N(E_t)$. Constraint (ii) may be deduced from the reduced K-matrix [11] for the channel $\pi\Sigma$, the only channel open below the $\bar{K}N$ threshold,

$$K^{(1)}(E) = K_\Sigma(E) - K_\Sigma(E)\frac{1}{1 + |k|\,K_N(E)}|k|\,K_\Sigma(E). \tag{17}$$

Since the $\pi\Sigma$ scattering phase takes the value $\pi/2$ at the pole of $K^{(1)}$, this constraint is

$$1 + |k(E_R)|(K_N(E_t) + (E_R - E_t)\rho_N) = 0. \tag{18}$$

Thus, the threshold K-matrix $K(E_t)$ is completely determined in terms of ρ_N by these constraints and the two parameters, ρ_Σ and ρ_Σ, are still free.

The situation for the M-matrix model (5) is quite similar. In terms of the matrix $M(E)$, the $\bar{K}N$ scattering length is given by

$$A_N(E)^{-1} = M_N(E) - \frac{M_\Sigma(E)^2}{M_\Sigma(E) - iq}. \tag{19}$$

The $\pi\Sigma$ scattering length below the $\bar{K}N$ threshold is real and takes the corresponding form

$$A_\Sigma(E)^{-1} = M_\Sigma(E) - \frac{M_\Sigma(E)^2}{M_N(E) - ik} \tag{20}$$

which takes the form

$$q\cot\delta = M_\Sigma(E) - \frac{M_\Sigma(E)^2}{M_N(E) + |k|} \tag{21}$$

below the $\bar{K}N$ threshold. The resonance energy E_R is given by the vanishing of (21) namely

$$(M_\Sigma(E_t) + R_\Sigma(E_R - E_t))(M_N(E_t) + R_N(E_R - E_t) + |k_R| = (M_\Sigma(E_t) + R_\Sigma(E_R - E_t))^2 \tag{22}$$

which is linear in $M_N(E_t)$, $M_\Sigma(E_t)$, R_N and R_Σ. Evaluating (19) at the $\bar{K}N$ threshold gives

$$b_0/a_0^2+b_0^2)=q_t M_X(E_t)^2/(q_t^2+M_\Sigma(E_t)^2) \tag{23a}$$

$$a_0/(a_0^2+b_0^2)=M_N(E_t)-(M_\Sigma(E_t)/q_t)(b_0/(a_0^2+b_0^2)). \tag{23b}$$

For assigned $M_\Sigma(E_t)$, $M_N(E_t)$ and $M_X(E_t)^2$ are determined from (23); for assigned R_X and R_Σ, R_N may be determined uniquely from (22). Hence, the scattering phase δ can be calculated, and the $\pi\Sigma$ mass distribution deduced, in terms of $M_\Sigma(E_t)$, R_X and R_Σ, using equation (21).

Quite an analogous procedure can be followed for the separable potential model (7). $T_N(E)$ can be obtained from the expression (8) for T_Σ, by replacing π, Σ, q and k by K, N, k and q, respectively. We note that both expressions are bilinear in s_N, s_Σ and $\sigma=(s_N s_\Sigma - s_X^2)$. At the $\bar{K}N$ threshold, the integrals $I_N(0)$ and $I_\Sigma(q_t)$ are known numbers, the former being real and the latter complex; equating $T_N(E_t)$ with the $\bar{K}N$ threshold scattering length $A_N(E_t)=a_0+ib_0$ gives two real linear equations for the real variables s_N, s_Σ and σ. Below the $\bar{K}N$ threshold, k takes the value $+i|k|$ and the integral $I_N(i|k|)$ is real. For the $\pi\Sigma$ resonance at $E=E_R$, equation (8) can be rewritten in the form

$$T_\Sigma^{-1}(E_R)=\Omega_\Sigma^{-1}(q_R)\{-I_\Sigma(q_R)+(1-s_N I_N(+i|k_R|))/(s_\Sigma-\sigma I_N(+i|k_R|)\}. \tag{24}$$

The resonance condition is that

$$\mathrm{Re}(T_\Sigma(E_R)^{-1})=0, \tag{25}$$

from which we obtain the third equation needed, the real equation

$$1-s_N I_N(+i|k_R|)-s_\Sigma\,\mathrm{Re}(I_\Sigma(q_R))+\sigma I_N(+i|k_R|)\,\mathrm{Re}\,I_\Sigma(q_R)=0. \tag{26}$$

The imaginary parts of the two sides of (24) are necessarily equal, as a consequence of unitarity; explicitly the identity is

$$\mathrm{Im}\,I_\Sigma(q)=(\omega_\pi(q)E_\Sigma(q)/\mu_\Sigma E)2\beta_\Sigma^3 q/(q^2+\beta^2)^2. \tag{27}$$

Thus, for specified $A_N(E_t)$ and resonance energy E_R, these three real equations can be solved uniquely for s_N, s_Σ and $\sigma=(s_N s_\Sigma - s_X^2)$, and the $(\pi\Sigma)^0$ mass spectrum then follows from (8), as a function of the potential shape parameters β_Σ and β_N.

Replacing the slowly varying integral over F in (3) by a constant C, the rate of the $\pi\Sigma$ events at energy E is given by

$$\frac{dN}{dE}=C\frac{\sin^2\delta}{k^2}\rho(k,Q) \tag{28}$$

where $\rho(k,Q)$ denotes the density of states for $\pi\Sigma$ total momentum Q and internal momentum k and we approximate it by

$$\rho(k,Q)\approx kQ \tag{29}$$

where Q is now the CM momentum for $\Sigma^*(1660)\rightarrow\pi\Lambda(E)$. Thus

$$\sin^2\delta=C(k/Q)(dN/dE), \tag{30}$$

where C must be adjusted to give $\sin^2\delta$ the value $+1$ at its peak. In other words, we assume that the Λ(1405) peak is resonant; we cannot demonstrate that this peak is necessarily due to a resonance, although it is the most plausible hypothesis. The

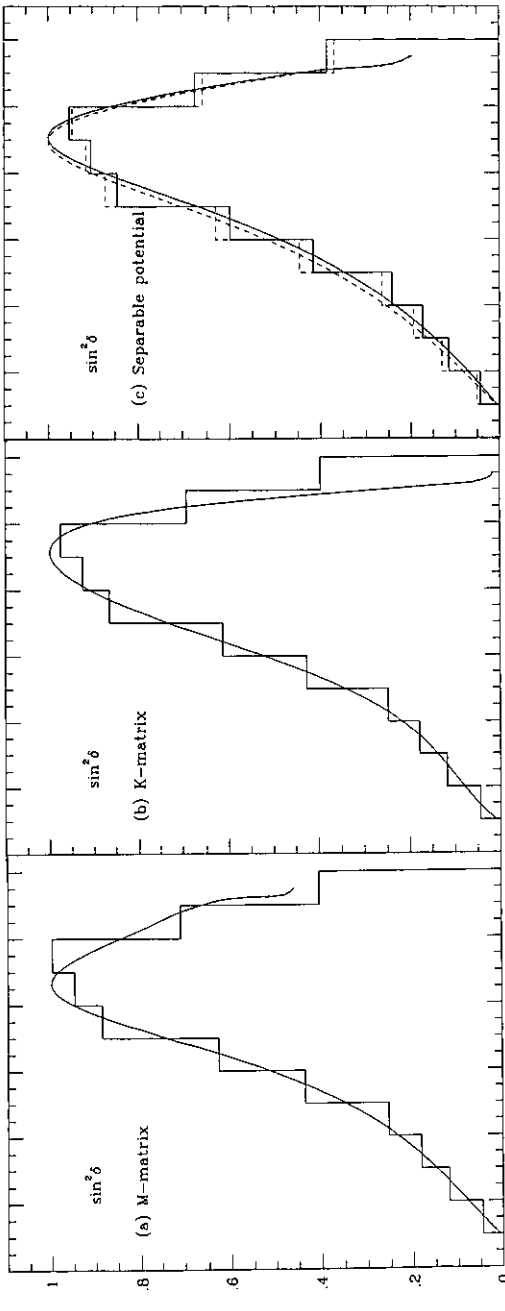

Figure 2. Hemingway's data from figure 1 is replotted to show it in relation to the calculated $\sin^2\delta$ for $\pi\Sigma$ scattering, for parametrization by (a) the M-matrix, (b) the K-matrix and (c) a Yamaguchi separable potential, the latter for relativistic kinematics (full curve) and non-relativistic kinematics (broken curve). The vertical scale has been adjusted to give $\sin^2\delta$ the value +1 at the resonance energy E_R; the adjustment is different for each case.

empirical data are presented in this way in figure 2. This makes it quite clear that, if there is a resonance, its energy E_R must lie in the vicinity of 1410 MeV.

4. The Λ(1405) parameters

Our procedure to fit Hemingway's data on the $\pi\Sigma$ mass spectrum was to calculate and minimize χ^2 for an assumed E_R, for the ten 10 MeV bins from 1330 to 1430 MeV. Note that the statistical error to be used for bin i is not simply $\sqrt{N_i}$, but $1.61\sqrt{N_i}$, as specified following his discussion of observational efficiencies. The least value $\chi^2(E_R)$ for fixed E_R is plotted as a function of E_R in figure 3, for the three models M, K and SR discussed above. For each model, our best estimate of E_R corresponds to the minimum of $\chi^2(E_R)$, the standard deviation σ_R being obtained by locating the values of E_R which correspond to the χ^2 value of $(\chi^2_{min} + 1)$, as indicated in figure 3. The values of E_R and σ_R are given in table 1, together with the best parameter set for each model.

The degree of dependence of E_R on the model is considerable, more than expected, and this makes it difficult for us to assign a firm value and standard error for E_R. We have expressed a strong preference for the model M, because of its success in a one-channel situation ($^3S_1$ np system) of the same kind (i.e. with interaction strength giving one bound state near a threshold). The standard deviation σ_R for M is much larger than those for K and SR, and this is a point in its favour. The round value $E_R = 1406.5 \pm 4.0$ MeV almost includes the best estimates of E_R for K and SR models, and it is the value we would recommend for use today.

We also made a direct search for the best fit for model SNR. It is remarkable that the $m(\pi\Sigma)$ spectrum for this case is almost indistinguishable from the best spectrum for model SR, as is shown in figure 1.

The best-fit $\sin^2\delta$ plots are compared with the data in figure 2. We note that the M-matrix fit shows a strongly downward S-shaped cusp at the threshold at $E_t = 1432$ MeV—the continued fall above E_t follows directly from unitarity, since

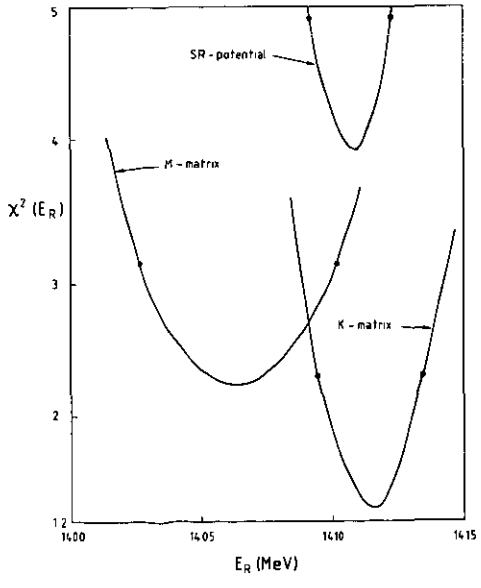

Figure 3. The lowest χ^2 obtained for each value of E_R is plotted against E_R for three parametrizations of the $\pi^-\Sigma^+$ mass distribution: the M-matrix (5), the K-matrix (6) and a Yamaguchi separable potential with relativistic kinematics. For each curve, the full circles indicate the values of E_R for which $\chi^2(E_R)$ is one unit above χ^2_{min} for that curve.

Table 1. Best-fit parameters, in turn, for the models M, K, SR and SNR discussed in the text, for the Hemingway ($\Sigma^+\pi^-$) mass distribution for $\Sigma(1660)^+ \to \pi^+(\pi^-\Sigma^+)$, below the K^-p threshold. The quantities ρ, K, M and β have units fm^2, fm, fm^{-1} and fm^{-1}, respectively: the quantities R and s are dimensionless

	M-matrix	K-matrix	SR potential	SNR potential
E_R	1406.4 MeV	1411.4 MeV	1410.8 MeV	1409.6 MeV
σ_R	3.9 MeV	2.0 MeV	1.5 MeV	—
χ^2_{min}/df	0.215	0.375	0.56	0.46
	$M_\Sigma(E_t) = -1.136$	$K_\Sigma(E_t) = -0.293$	$s_\Sigma = -0.003$	$s_\Sigma = -0.020$
	$M_\Lambda(E_t) = 1.254$	$K_\Lambda(E_t) = 0.929$	$s_\Lambda = 0.320$	$s_\Lambda = 0.433$
	$M_N(E_t) = 1.69$	$K_N(E_t) = -1.739$	$s_N = 0.946$	$s_N = 1.089$
	$R_\Sigma = 19.92$	$\rho_\Sigma = 14.700$	$\beta_\Sigma = 1.173$	$\beta_\Sigma = 1.768$
	$R_\Lambda = -6.65$	$\rho_\Lambda = -3.625$	$\beta_N = 5.405$	$\beta_N = 6.298$
	$R_N = 3.346$	$\rho_N = -0.167$		
$E^*, \Gamma/2$(MeV)	1404.9, 26.6	1387, 39.8	1526.0, 158.8	1417.0, 28.5
Γ_u, Γ_l(MeV)	27.1, 24.6	16.0, 32.6	18.0, 30.0	18.0, 30.0

the new $\bar{K}N$ channel is in competition with the $\pi\Sigma$ channel—whereas the K-matrix fit shows almost no cusp at all. The latter is related with the fact that $\delta(E_t)$ is almost zero in the linear K-matrix fit. The SR fit is rather intermediate, in this respect.

We note here that the 1430–40 bin shown in figures 1 and 2 was not included in our fitting. It was omitted in order to avoid the complications of the split $\bar{K}N$ thresholds (K^-p and $\bar{K}^0n$), whose proper treatment would require the introduction of an $I = 1$ scattering length at least. In essence, our discussion has assumed isospin conservation, with a single $\bar{K}N$ threshold at the physical K^-p threshold. The two bins for 1430–50 suggest that the empirical rate falls abruptly above the threshold, but is substantial at threshold. This is quite contrary to expectation for model K and is an additional argument against it.

The definition of a width for this resonance is not unambiguous. The location of a corresponding pole in the S-matrix, at some point $(E^* - i\Gamma/2)$ on sheet II of the E plane, could have been a natural choice. The values $(E^*, \Gamma/2)$ of the pole are given in table 1 for each model we have considered. For the model M, the values are reasonable, $E^* = 1404.9$ MeV and $\Gamma = 53.1$ MeV. The width of the calculated resonance curve shown in figure 2 could be defined by the energy values at which $\delta = 45°$ and 135°, in other words by full width at half maximum; despite the strong asymmetry of the resonance peak, the upper and lower half widths are almost the same, since $\Gamma_u/2 = 27.1$ MeV and $\Gamma_l/2 = 24.6$ MeV, and give a full width $\Gamma = (\Gamma_u + \Gamma_l)/2 = 51.7$ MeV, close to the value given by the pole location. This is much less the case for models K and SR, where the location of E^* is far from E_R; the calculated peaks for them are quite asymmetric, with (Γ_u, Γ_l) equal to (32.0, 65.2) for K and (36, 60) for SR. It is noteworthy that the poles for SR and SNR have quite different locations, even though their mass distributions are almost indistinguishable; of course these two models have different kinematics.

5. Discussion and conclusion

The sensitivity of the M-model fit to $\bar{K}N$ threshold amplitude, used as our constraint (ii), is a question which needs consideration, since there have been some consider-

Table 2. Fits to the Hemingway data for a number of values of $A_N(E_t) = a_0 + ib_0$ with a_0, b_0 in the range $(1.54 \pm 0.5, 0.74 \pm 0.2)$ fm. $E^* - i\Gamma/2$ is the location of the nearby pole on sheet II.

a_0 (fm)	b_0 (fm)	E_R (MeV)	χ^2/df	E^* (MeV)	$\Gamma/2$ (MeV)
−1.04	0.54	1409.0	1.41	1400.7	32
−2.04	0.54	1409.7	0.34	1413.5	16
−1.54	0.74	1406.4	0.215	1404.9	27
−2.04	0.74	1407.6	0.84	1410.2	24
−1.04	0.94	1404.3	1.13	1397.2	26
−2.04	0.94	1407.1	0.33	1405.8	28

able variations in the value obtained for $(a_0 + ib_0)$ by different low-energy $\bar{K}N$ analyses in the past [5–10]. The best-fit parameters we have obtained for Λ(1405) with the *M*-matrix, for various threshold lengths (a_0, b_0) in the range $(1.51 \pm 0.50, 0.74 \pm 0.20)$ fm are given in table 2. The χ^2/df obtained is not important for us, other than giving a rough measure on the quality of the fit, since we do *not* seek, and would not wish *to determine* $(a_0 + ib_0)$ in this way. The E_R values range from 1406 to 1410 MeV and the 'pole widths' $\Gamma/2$ from 16 to 32 MeV; they are not all equally good fits to the $m(\pi\Sigma)$ data. The UCL scattering length $(-1.04 + i0.54)$ fm obtained [9, 10] from data at and above the $\bar{K}N$ threshold lies at the extreme boundary of the region we considered; such a small value as $a_0 = -1.04$ fm gives us some difficulty in fitting the below-threshold data.

The lack of full data on reaction (1*b*) is unfortunate. The two π^+ mesons emitted have comparable energy values and the interference between them could be quite strong in the final state $\pi^+\pi^+\Sigma^-$, which could perhaps have given us additional information about the $\Sigma^*(1660) \rightarrow \pi\Lambda(1405)$ decay process. Analysis of the final state $\pi^-\Sigma^+$ of Λ(1405) by itself allows the possibility of distortions arising from background non-resonant $\pi^-\Sigma^+$ states with $I = 1$, due to $\Sigma^*(1660) \rightarrow \pi(\pi^-\Sigma^+)$. Ideally, it would be desirable to analyse $\pi^\mp\Sigma^\pm$ states at the same time, since ($I = 0$, $I = 1$) interference terms could then be eliminated, in large measure.

Model *M* leads quite naturally to a strong S-shaped cusp and a very asymmetric resonance peak. However, model *K* gives an acceptable fit without any appreciable cusp behaviour, so that it may be questionable to insist that the data demonstrate the existence of a cusp. Model *K* has fitted the rapid fall in rate as $E \rightarrow E_t$ from below by having a small value for $K_\Sigma(E_t)$, which means that since $\delta(E_t) = \tan^{-1}(q_t K_\Sigma(E_t))$ is small, the value of $\sin^2\delta$ at threshold is very small. Of course, in that case, Watson's approximation is questionable, but the prediction of a low rate there should still hold, even if the magnitude is not precisely correct. The gross underestimate of the rate for the 1430–40 bin is a serious argument against model *K*. To demonstrate empirically the presence of this cusp, much larger statistics, perhaps by a factor of ten, will be needed, with good precision for the measurement of $E(\pi\Sigma)$ for each event.

The properties of Λ(1405) could be determined from the study of $\Sigma^*(1660) \rightarrow \pi\Lambda(1405)$ for $\Sigma^*(1660)$ resulting from other reaction processes. The most direct process would be $\Sigma^*(1660)$ formation by a K^- beam of about 750 MeV c^{-1} incident on a hydrogen target. Although this reaction is well known, its three-body states $\Sigma\pi\pi$ have not yet been studied in any high-statistics electronic experiment. The bubble chamber data at 750 MeV c^{-1} give low branching fractions for $\Sigma^*(1660) \rightarrow$

$\pi\Lambda(1405)$, being respectively, <6% as reported by Armenteros *et al* [15] and $7 \pm 4\%$ reported by Brucker *et al* [16]; these low values are disconcerting because they do not square with the prominence of this channel in the high-energy production data. In fact, Timmermans *et al* [17] have raised doubts concerning the relationship between the $\Sigma^*(1660)$ states produced in their study of K^-p reactions for incident K^- momentum 4.2 GeV c^{-1} at large and at small momentum transfer values and the $\Sigma^*(1660)$ formed directly in the K^-p reaction at 750 MeV c^{-1}. Unfortunately, it appears likely that there is more than one Σ^* resonance in the vicinity of 1660 MeV and that the uncertainties concerning them will need to be resolved, before other $\Sigma^*(1660)$ data can be used to provide another source of $\Lambda(1405)$ events. Hemingway's study of $\Lambda(1405)$ was based on the small momentum transfer events, so that the $\Sigma^*(1660)$ state he used is probably not that formed in K^-p collisions at 750 MeV c^{-1}. He also noted that the Σ^{*+} peak in $\Sigma^+\pi^-\pi^+$ final states has a different shape from that for $\Sigma^-\pi^+\pi^+$ final states, which suggests that there is interference between the $\Lambda(1405)\pi^+$ and some non-resonant $I = 1$ S-wave $(\pi\Sigma)$ states which contribute to these $(\Sigma\pi)^0\pi^+$ final states.

Other production processes for $\Lambda(1405)$ are known which do not involve $\Sigma^*(1660)$. The best known is the study of the reaction

$$\pi^- + p \rightarrow K^0 + \Lambda(1405) \rightarrow K^0 + (\pi^{\mp}\Sigma^{\pm}) \tag{31}$$

by Thomas *et al* [18] at 1.69 Gev c^{-1}. This final state has the advantage that the K^0 does not have a strong interaction with baryons, nor with the π^- meson; the $K^0\pi^+$ interaction is resonant at CM energy 891 MeV but this resonance effect lies beyond the region studied. Their $\pi^{\pm}\Sigma^{\mp}$ spectrum peaks at the same energy as Hemingway's but has a somewhat different fall-off as $E(\pi\Sigma)$ approaches the KN threshold, without visible cusp there. On the other hand, Thomas *et al* have a few events (about 300) more than an order of magnitude below those of Hemingway, so that all available events had to be used; there was no rigorous selection of events, to clear out backgrounds to the $\Lambda(1405)$ region studied.

Hemingway's data can also be compared directly with theoretical predictions of the $\pi\Sigma$ interaction, rather than proceeding through the identification of a resonant state and the determination of its parameters. The most serious candidate theory is the chiral cloudy bag model [19], which finds that $\Lambda(1405)$ is a superposition of three-quark and $\bar{K}N$ configurations, but mostly ($\simeq$90%) the latter. The CBM prediction is plotted in figure 4 of Hemingway's paper; it is quite similar to the curve for the *K*-matrix model, shown in figure 1 here.

Acknowledgment

We wish to thank Dr R Hemingway warmly for his determining the $(\pi\Sigma)$ spectrum, at our suggestion, for the $\Sigma^{\pm}\pi^{\mp}\pi^+\pi^-$ events found and processed by the Amsterdam–CERN–Nijmegen–Oxford Collaboration from their exposure of the CERN 2 m hydrogen bubble chamber to a 4.2 GeV c^{-1} K^- beam, long after the experimental analysis was completed, in fact long after the collaboration had dissolved.

Appendix. Evaluation of the dispersion integral $I(E)$

We consider the integral

$$I(E)=\frac{2\beta^3}{\pi\mu}\int_0^\infty \frac{k^2\,\mathrm{d}k}{(k^2+\beta^2)^2}\cdot\frac{1}{\omega(k)+E(k)-E-\mathrm{i}\varepsilon} \tag{A1}$$

for a meson(m)-baryon(M) system, where μ is their reduced mass, $\omega(k)=(m^2+k^2)^{1/2}$ and $E(k)=(M^2+k^2)^{1/2}$. In the non-relativistic limit for both particles, the integral takes the form

$$I_{\mathrm{NR}}(E)=\frac{4\beta^3}{\pi}\int_0^\infty \frac{k^2\,\mathrm{d}k}{(k^2+\beta^2)^2}\cdot\frac{1}{(k^2-p^2-\mathrm{i}\varepsilon)}=\frac{1}{(1-\mathrm{i}p/\beta)^2} \tag{A2}$$

where p is the CM momentum for total energy E, so that $\omega(p)+(E(p)=E$.

The last factor for expression (A1) can now be written in the form

$$\left(\frac{1}{\omega(k)+E(k)-\omega(p)-E(p)-\mathrm{i}\varepsilon}-\frac{2\omega(p)E(p)}{E(k^2-p^2-\mathrm{i}\varepsilon)}\right)+\frac{2\omega(p)E(p)}{E}\cdot\frac{1}{(k^2-p^2-\mathrm{i}\varepsilon)} \tag{A3}$$

in which the first bracket is non-singular at $p=k$, while the last term is explicitly integrable (cf (A2)). In expression (A1), this latter term leads to the result

$$\frac{\omega(p)E(p)}{\mu E}\left(\frac{\beta^2(\beta^2-p^2)}{(p^2+\beta^2)^2}+\mathrm{i}\frac{2p\beta^3}{(p^2+\beta^2)^2}\right). \tag{A4}$$

The large bracket of (A3) is readily brought to the following real and non-singular form, symmetric between the functions ω and E,

$$\left(\frac{\omega(p)}{E}\frac{\omega(k)+\omega(p)}{E(k)+E(p)}+\frac{E(p)}{E}\frac{E(k)+E(p)}{\omega(k)+\omega(p)}\right)\frac{1}{(E(k)+\omega(k)-E)}. \tag{A5}$$

This is in a form convenient for the numerical integration of (A1) over k; its convergence can be improved by subtracting $1/k$ from (A5) since the integral of this subtracted term is simply $\beta/2\pi\mu$. The form (A5) can be continued below the threshold $(M+m)$ by the replacement of p by $+\mathrm{i}|p|$ in (A5). At the threshold, $p=0$ and the value of $I(E_t)$ consists of (A4), which is $+1$ for $p=0$, plus the integral (A1) taken over the expression (A5) which is non-zero and positive.

A useful analytical approximation to (A1) in this work has been the replacement of $E(k)$ by its non-relativistic approximation $(M+k^2/2M)$. The integral (A1) may then be cast into the semirelativistic form

$$\mathrm{I}_{\mathrm{SR}}(E)=\frac{2\beta^3}{\pi\mu}\int_0^\infty \frac{k^2\mathrm{d}k}{(k^2+\beta^2)^2}\cdot\frac{1}{(k^2-p^2)}\left(\frac{1}{(\omega(p)+\omega(k))^{-1}+(2M)^{-1}}\right) \tag{A6}$$

which can be conveniently regularized by subtracting the integral

$$\frac{2\beta^3}{\pi\mu}\int_0^\infty \frac{k^2\,\mathrm{d}k}{(k^2+\beta^2)^2}\frac{1}{(k^2-p^2)}\left(\frac{2\omega(p)M}{M+\omega(p)}\right)=\frac{\omega(p)}{m}\frac{(M+m)}{(M+\omega(p))}\frac{1}{(1-\mathrm{i}p/\beta)^2}. \tag{A7}$$

The large brackets of (A6) and (A7) combine to give

$$\frac{2M(\omega(p)+\omega(k))}{2M+\omega(p)+\omega(k)}-\frac{2\omega(p)M}{M+\omega(p)}=\frac{k^2-p^2}{M+\omega(p)}\left(\frac{2M^2}{(\omega(k)+\omega(p)+2M)(\omega(k)+\omega(p))}\right) \tag{A8}$$

which cancels the singularity in the integrand of (A6). After breaking the large bracket of (A8) into partial fractions, the integral I_{SR} consists of three forms:

$$I_{SR}(E) = \frac{\omega(p)}{m} \cdot \frac{M+m}{(M+\omega(p))} \left(\frac{1}{(1+ip/\beta)^2} + \frac{4\beta^2}{\pi} \cdot \frac{M}{\omega(p)} [J(\omega(p)) - J(2M+\omega(p))] \right) \tag{A9}$$

where

$$J(\omega(z)) = \int_0^\infty \frac{k^2\,dk}{(k^2+\beta^2)^2} \frac{1}{\omega(k)+\omega(z)} \tag{A10}$$

$$= \frac{1}{(z^2+\beta^2)^2} \left\{ -\tfrac{1}{2}\omega(p)\beta^2(\beta^2-z^2) + \frac{\beta^3}{\pi} \left[\beta^2 + z^2 + z\omega(z) \ln\left(\frac{\omega(z)-z}{\omega(z)+z}\right) \right.\right.$$

$$\left.\left. + B(\beta)[\tfrac{1}{2}m^2(\beta^2-p^2) + p^2\beta^2] \right] \right\} \tag{A11}$$

where the function $B(\beta)$ is given by

$$B(\beta) = \frac{1}{\beta^2} \frac{1}{(\beta^2-m^2)^{1/2}} \tfrac{1}{2} \ln\left(\frac{\beta + (\beta^2-m^2)^{1/2}}{\beta - (\beta^2-m^2)^{1/2}}\right) \tag{A12}$$

for real $\beta > m$, its value for $\beta \leqslant m$ to be obtained from this by analytical continuation. The expression (A11) holds as it stands, for $E > (M+m)$. It also holds below threshold if the replacement $p \rightarrow +i|p|$ is made, as long as $|p| \leqslant m$.

References

[1] Particle Data Group 1990 *Phys. Lett.* **239B** 78–81
[2] Hemingway R J 1984 *Nucl. Phys.* B **253** 742
[3] Watson K M 1952 *Phys. Rev.* **85** 852
[4] Dalitz R H and Deloff A 1990 The analysis of low-energy KN reaction data. In preparation
[5] Kim J K 1967 *Phys. Rev. Lett.* **19** 1074
[6] Martin A D 1980 *Workship on Low and Intermediate Kaon–Nucleus Physics* ed E Ferrari and G Violini (Dordrecht: Reidel) p 97
[7] Martin A D 1981 *Nucl. Phys.* B **179** 33
[8] Chao Y A, Kraemer R W, Thomas D W and Martin B R 1973 *Nucl. Phys.* B **56** 46
[9] Miller D J 1984 *Intersections Between Particle and Nuclear Physics* (*Steamboat Springs, 1984*) (AIP Conf. Proc. 123) ed R E Mischke (New York: AIP) pp 783–798
[10] Conboy J E 1985 *Rutherford Appleton Laboratory Report* RAL-85-091
[11] Dalitz R H and Tuan S F 1960 *Ann. Phys., NY* **3** 307
[12] Ross M and Shaw G 1960 *Ann. Phys., NY* **9** 391; 1961 *Ann. Phys., NY* **13** 147
[13] Blatt J M and Weisskoff V F 1952 *Theoretical Nuclear Physics* (New York: Wiley) p 62
[14] Torres M, Dalitz R H and Deloff A 1986 *Phys. Lett.* **174B** 213
[15] Armenteros R *et al* 1968 *Phys. Lett.* **28B** 521
[16] Brucker E B *et al* 1970 *Hyperon Resonances-70*, ed E C Fowler (Durham, NC: Moore) p 155
[17] Timmermans J J M *et al* 1976 *Nucl. Phys.* B **112** 77
[18] Thomas D W, Engler A, Fisk H E and Kraemer R W 1973 *Nucl. Phys.* B **56** 15
[19] Veit E A, Jennings B K, Thomas A W and Barrett R C 1985 *Phys. Rev.* D **31** 1033
[20] Siegel P B and Weise W 1988 *Phys. Rev.* C **38** 2221